

pubs.acs.org/acsaenm Article

Surfactant-Modified Clay for Adsorption of Mixtures of Per- and Polyfluoroalkyl Substances (PFAS) in Aqueous Solutions

Tao Jiang,* Weilan Zhang, Aswin Kumar Ilango, Jeremy I. Feldblyum, Zheng Wei, Haralabos Efstathiadis, Mehmet V. Yigit, and Yanna Liang



Cite This: https://doi.org/10.1021/acsaenm.2c00096



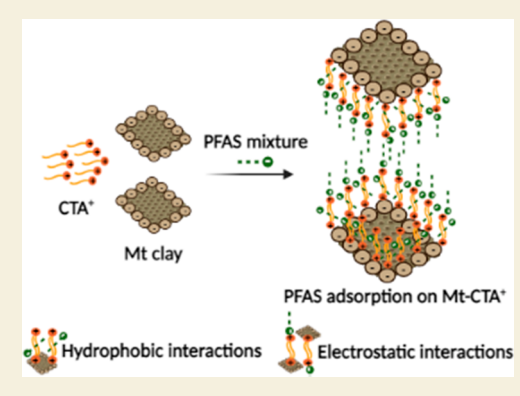
ACCESS I

III Metrics & More

Article Recommendations

s Supporting Information

ABSTRACT: Per- and polyfluoroalkyl substances (PFAS) are persistent, bioaccumulative, and ubiquitous contaminants that are harmful to both humans and ecosystem health. To remove PFAS effectively and efficiently from the aqueous environment, a clay-based adsorbent was synthesized via the modification of montmorillonite by a cationic surfactant cetyltrimethylammonium chloride (CTAC). Through the coexposure adsorption tests with organic dyes and PFAS mixtures, the optimal ratio of CTAC to cation exchange capacity (CEC) was identified. The optimal modified clay exhibited drastically improved adsorption performance, achieving 100% removal efficiency of the PFAS mixture consisting of nine short- and long-chain PFAAs, GenX, and three precursors at initial concentrations of the parts per billion (ppb) level. Additionally, the modified clay outperformed other commercial adsorbents with respect to adsorption performance. The adsorption kinetic data of all PFAS, which were well



described by the pseudo-second-order model, suggested an expeditious adsorption process and an adsorption behavior dependent on the initial concentration and carbon chain length. Among the three examined adsorption isotherms, the Sips model combining Langmuir and Freundlich models showed the best fitting correlation, indicating that multiple interactions might be involved in the adsorption process. This hypothesis was supported by characterizations showing that the modified clay possessed physicochemical properties favorable for electrostatic interactions and hydrophobic interactions.

KEYWORDS: montmorillonite, modification, surfactant, poly- and perfluoroalkyl substances, PFAS precursors, adsorption

1. INTRODUCTION

Per- and polyfluoroalkyl substances (PFAS) are a group of synthetic organic compounds in which the hydrogen atoms bound to the carbon backbones are fully or partially substituted with fluorine. The unique properties of PFAS have enabled their widespread use in numerous industrial processes and commercial products.² The wide usage of PFAS results in their broad distribution and possible adverse effects in the environment.³⁻⁵ Lately, the U.S. EPA dramatically lowered the lifetime health advisory levels in drinking water for perfluorooctanoic acid (PFOA) and perfluorooctanesulfonic acid (PFOS), from the previous 70 parts per trillion (ppt) to 0.004 ppt for PFOA and 0.02 ppt for PFOS.6 Additionally, for the first time, the EPA issued final health advisories for two PFOA and PFOS alternatives, namely undecafluoro-2-methyl-3-oxahexanoic acid (GenX) and perfluorobutanesulfonic acid (PFBS), in drinking water. Therefore, it is critical and urgent to remove PFAS from the environment. However, due to the remarkably high energy of the carbon-fluorine bonds, PFAS are resistant to thermal, chemical, and biological decomposition, leading to their extreme stability and persistence. Thus, the destruction of PFAS is extraordinarily difficult. Even an intensive energy input may still be ineffective for the

destruction of PFAS.^{8,9} Moreover, conventional water and wastewater treatment processes such as coagulation, flocculation, sedimentation, and filtration have been demonstrated to be ineffective for PFAS removal from aqueous sources.⁹ Adsorption, on the other hand, is an effective way to tackle PFAS contamination from water,¹⁰ sludge,¹¹ and soil.¹²

Adsorbents for PFAS mainly include carbon-based materials, ^{11,13} ion exchange resins, ^{14,15} biosorbents, ¹⁶ and clay-based materials. ^{17,18} Activated carbons (ACs), including granular and powdered AC (GAC and PAC), carbon nanotubes (CNTs), and biochar, are the main carbon-based materials for PFAS adsorption, ¹⁰ of which powdered AC and CNTs showed high adsorption capacities. ^{19,20} The nonpolar functional groups of carbon-based adsorbents contribute to hydrophobic PFAS adsorption. ²¹ Carbon-based materials, however, have encountered two critical issues that are well-recognized: namely, slow

Received: August 31, 2022 Accepted: October 12, 2022 Published: October 20, 2022



Table 1. Physicochemical Properties of PFAS Investigated in This Study^a

category	compound	abbreviation	chemical formula	mol wt (g/mol)	$S_{\rm w}$ (25 °C)	pK _a (25 °C)		
short-chain PFCA	perfluorohexanoic acid	PFHxA	$C_6HF_{11}O_2$	314	15.7 ³⁶	-0.16^{37}		
short-chain PFCA	perfluoroheptanoic acid	PFHpA	$C_7HF_{13}O_2$	364	3.65×10^{-338}	-2.29^{38}		
long-chain PFCA	perfluorooctanoic acid	PFOA	$C_8HF_{15}O_2$	414	3.4 ³⁶	-0.2^{37}		
long-chain PFCA	perfluorononanoic acid	PFNA	$C_9HF_{17}O_2$	464	6.25×10^{-238}	-0.21^{38}		
long-chain PFCA	perfluorodecanoic acid	PFDA	$C_{10}HF_{19}O_2$	514	9.5 ³⁹	-5.2^{40}		
long-chain PFCA	perfluoroundecanoic acid	PFUnA	$C_{11}HF_{21}O_2$	564	4×10^{-339}	-5.2^{40}		
short-chain PFSA	potassium perfluorobutanesulfonate	PFBS	$C_4F_9O_3SK$	338	46.2 ¹⁷	0.14^{37}		
long-chain PFSA	perfluorohexanesulfonic acid potassium salt	PFHxS	$C_6F_{13}KO_3SK$	438	2.3^{39}	0.14^{37}		
long-chain PFSA	heptadecafluorooctanesulfonic acid potassium salt	PFOS	$C_8HF_{17}KO_3SK$	538	0.57^{36}	-3.27^{41}		
PFOA alternative	undecafluoro-2-methyl-3-oxahexanoic acid	GenX	$C_6HF_{11}O_3$	330	N/A	2.84 ⁴⁰		
precursor	6:2 fluorotelomer sulfonic acid	6:2 FTSA	$C_8H_5F_{13}O_3S$	428	1.3 ³⁹	1.31^{39}		
precursor	2-N-ethyl perfluorooctane sulfonamido acetic acid	N-EtFOSAA	$C_{12}H_8F_{17}NO_4S$	585	N/A	N/A		
precursor	8:2 fluorotelomer phosphate diester	8:2 diPAP	$C_{20}H_9F_{34}O_4P$	990	N/A	N/A		
^a Definitions: S_w , solubility in water, g/L; p K_a , dissociation constant; N/A, data not available.								

adsorption kinetics and much lower efficiency in removing short-chain PFAS than long-chain ones.²² Additionally, it is unclear at this stage whether these materials are able to retain PFAS precursors that have attracted increasing concerns in recent years³ in aqueous solutions. Furthermore, the process of producing carbon-based materials is highly energy intensive

and has drawn scrutiny and attention recently in terms of greenhouse gas emissions.²² Compared to carbon-based materials, ion exchange resins have been reported to be less cost-effective²³ and biosorbents exhibited lower adsorption capacity.¹³

Clay-based materials are another category of PFAS adsorbent. A variety of natural clays have been studied for PFAS adsorption, such as montmorillonite, 24,25 kaolinite, 24,25 boehmite,²⁶ hematite,²⁵ and alumina.²⁷ However, the hydration of inorganic cations at the exchange sites in natural clays leads to their negative charge and hydrophilic surface and thus low effectiveness for adsorption of hydrophobic and anionic PFAS.²¹ Consequently, conversion of the hydrophilic surface to a lipophilic surface by modifying natural clays with surfactants is a strategy for enhancing PFAS adsorption. After modification, the hydrophobic alkyl chains of surfactants would enhance PFAS adsorption via hydrophobic partitioning.21 Moreover, the positively charged surfaces generated from modification by cationic surfactants have an affinity to anionic PFAS through electrostatic interactions.²⁸ Several commercial clay-based PFAS adsorbents have been available on the market, such as FLUORO-SORB and matCARE.

As a member of the smectite group, montmorillonite (Mt) has a structure composed of two tetrahedral silicate layers sandwiching an aluminum oxide/hydroxide layer (2/1 layered structure). This structure enables a high cation exchange capacity (CEC) and specific surface area. 30 To modify its intrinsically hydrophilic surface for enhancing PFAS adsorption, Mt has been amended with quaternary ammonium compounds in previous studies. For example, Zhou et al.¹⁷ modified Mt with the cationic surfactant hexadecyltrimethylammonium bromide (HDTMAB) to improve PFOS adsorption in aqueous solutions and achieved an adsorption capacity of approximately 339 mg/g for the modified clay with a HDTMAB/CEC ratio of 0.5. Wang et al.³¹ amended Mt with the quaternary ammonium compounds L-carnitine and choline, and the adsorption of PFOA, PFOS, GenX, and PFBS was largely enhanced compared to the original Mt. These two studies both focused on a very limited number of PFAS. Given

the fact that PFAS oftentimes exist in the environment as a mixture of multiple compounds, 4,11 adsorbents that are robust and versatile toward adsorbing all types of PFAS (e.g., short-and long-chain perfluoroalkyl acids (PFAAs) as well as PFAA precursors) are highly desired. Such adsorbents have not been reported in the literature.

In this study, we synthesized a Mt-based adsorbent through modification of Mt K10, which is extensively used as an environmentally benign catalyst for organic reactions,³² by the cationic quaternary ammonium compound cetyltrimethylammonium chloride (CTAC). The adsorbent was then characterized by analytical instruments. The PFAS mixture for adsorption experiments consisted of GenX and nine PFAAs with high occurrence in the environment,³³ including six perfluorocarboxylic acids (PFCAs) with carbon chain lengths from 6 to 11 (i.e., perfluorohexanoic acid (PFHxA), perfluoroheptanoic acid (PFHpA), PFOA, perfluorononanoic acid (PFNA), perfluorodecanoic acid (PFDA), and perfluoroundecanoic acid (PFUnA)), and three perfluorosulfonic acids (PFSAs) with carbon chain lengths from 4 to 8 (i.e., perfluorobutanesulfonate (PFBS), perfluorohexanesulfonate (PFHxS), PFOS). Three frequently detected PFAA precursors in the environment, 34 i.e., 6:2 fluorotelomer sulfonic acid (6:2 FTSA), 2-N-ethyl perfluorooctane sulfonamido acetic acid (N-EtFOSAA), and 8:2 fluorotelomer phosphate diester (8:2 diPAP), were also included in the PFAS mixture for adsorption tests. Moreover, two organic dyes, namely methylene blue (MB) and rose bengal (RB), were added to the PFAS mixture in the initial adsorption experiments to facilitate selection of the optimal CTAC/CEC ratio and to examine the impacts of the potential presence of other organic pollutants on PFAS adsorption. The adsorption performance, including removal efficiency and adsorption kinetics and isotherms, for short- and long-chain PFAAs, GenX, and precursors was evaluated. Finally, the modified clay was compared with other commonly used adsorbents with respect to adsorption performance.

2. MATERIALS AND METHODS

2.1. Chemical Reagents and Analysis of PFAS

The information for chemical reagents used in this study can be found in Table S1. The physicochemical properties of PFAS investigated in this study are shown in Table 1. Prior to quantification, samples collected in the adsorption experiments were subject to centrifugation at 14000g for 10 min. The supernatant was then spiked with $^{13}C_4$ -PFOS and $^{13}C_2$ -PFOA as internal standards according to EPA

Table 2. Initial pH and Concentration of each PFAS (C_0, ppb) at Each Level of Mixtures in Adsorption Kinetic and Isotherm Experiments

	concentration (ppb)												
	PFHxA	PFHpA	PFOA	PFNA	PFDA	PFUnA	PFBS	PFHxS	PFOS	GenX	6:2 FTSA	N-EtFOSAA	pН
level 1	49.1	40.5	30.7	41.3	34.2	12.3	9.9	6.7	5.7	8.2	6.3	0.4	5.06
level 2	101.8	88.5	66.5	87.9	74.7	33.6	20.1	14.0	12.0	16.8	11.7	1.8	4.60
level 3	260.9	226.1	171.2	222.6	179.1	70.1	50.9	35.5	30.7	40.5	30.6	3.0	5.10
level 4	1088.1	987.2	729.8	910.9	558.1	268.8	209.1	153.5	138.4	158.6	127.1	16.8	4.90
level 5	2699.3	2495.9	1820.4	1885.4	1121.2	960.2	516.8	382.4	357.8	372.4	357.5	259.3	5.08

Method 537.1 Revision 2.0. Target PFAS in the prepared samples were quantified by a 1290 Infinity II LC system coupled with a 6470 Triple Quad Mass Spectrometer (LC-MS/MS, Agilent Technologies, Santa Clara, CA, USA). Two Agilent Eclipse Plus C18 columns, including a ZORBAX analytical column (3 \times 50 mm, 1.8 μ m) and a delay column (4.6 \times 50 mm, 3.5 μ m), were employed with a working temperature of 50 °C. A binary mobile phase with solvents A and B of 5 mM ammonium acetate in water and 95% methanol, respectively, was used at a flow rate of 0.5 mL/min. The content of solvent A in the mobile phase gradient profile began at 70%, decreased to 0% at 8 min, was held at 0% for 4 min, and reverted back to the initial value over the course of 12 min. More information on LC-MS/MS measurement conditions can be found in our previous studies 8,12,35 and Table S2.

2.2. Synthesis of Modified Clay

Montmorillonite K10 (granules with ≥80% ranging from 0.5 to 1.25 mm; Alfa Aesar, Haverhill, MA, USA) with a cation exchange capacity (CEC) of 59 mmol/100 g⁴² was used for the synthesis of cetyltrimethylammonium chloride (CTAC) modified clay. A twostep procedure similar to what was described in previous publications^{17,30} was employed in the synthesis process. Briefly, 100 g of K10 Mt was added to a Na2CO3 solution in a flask, and the mixture was stirred at 800 rpm at room temperature for 3 h. Then a few drops of concentrated hydrochloric acid were added to the solution, followed by rinsing with deionized (DI) water three times until no Cl was detectable. The pellet was dried at 108 °C overnight, which generated the solid of sodium montmorillonite (Na-Mt). The obtained Na-Mt is termed as unmodified clay in the following sections. The unmodified clay was then added to a 10, 25, or 100 mmol/L solution of CTAC, and the mixtures were stirred at 800 rpm at 80 °C for 2 h, followed by rinsing with DI water three times and drying at 108 °C for 10 h. Consequently, the process generated three types of modified clays with different CTAC/CEC ratios, i.e., 0.34, 0.85, and 3.39, which are referred to as Mt-CTAC_{0.34}, Mt-CTAC_{0.85}, and Mt-CTAC_{3.39}, respectively.

2.3. Characterization of Adsorbents

The morphological and compositional analyses of the unmodified (Na-Mt) and CTAC-modified clays were performed with a scanning electron microscope equipped with energy dispersive X-ray spectroscopy (SEM-EDS, Zeiss LEO 1550, Oberkochen, Germany; Bruker Quantax XFlash 6, Billerica, MA, USA). A Rigaku MiniFlex 6G benchtop powder X-ray diffractometer (XRD, Rigaku Corporation, Tokyo, Japan) was used to examine the crystal structure of clays using Cu K α radiation. The surface area and pore volume of the adsorbents were determined by the Brunauer–Emmett–Teller (BET) method⁴³ using a 3Flex gas adsorption analyzer (Micromeritics, Norcross, GA, USA). Three activation temperatures, i.e., room temperature (ca. 23 °C), 100 °C, and 200 °C, were employed to activate the samples at reduced pressure (ca. 0.1 mbar) for 24 h before N₂ gas adsorption analysis.

The ζ potentials of Na-Mt and Mt-CTAC_{0.85} at the original pH and adjusted pH in the range of 0–12 were measured to quantify the adsorbent surface charge using a Malvern Zetasizer Nano-ZS analyzer (Malvern Panalytical Ltd., Malvern, UK). The pH at the point of zero charge (pH_{PZC}) was determined as the pH at which the ζ potential was equal to 0. The infrared spectra of samples were obtained using a PerkinElmer Spectrum 100 Fourier transform infrared (FTIR)

spectrometer (Waltham, MA, USA). Four samples were evaluated, including Na-Mt, pristine Mt-CTAC $_{0.85}$, and two spent Mt-CTAC $_{0.85}$ samples generated from the kinetic experiments after exposure to PFAS mixtures for 24 h. More experimental details about the adsorbent characterization can be found in Text S1 in the Supporting Information.

2.4. Adsorption Experiments

All adsorption experiments were performed in a batch mode and in triplicate. A coexposure adsorption test with a mixture of the 10 PFAS (Table 1) and one of two organic dyes, either MB or RB (Figure S1), was used to evaluate the adsorption performance of Na-Mt, Mt-CTAC $_{0.34}$, Mt-CTAC $_{0.85}$, and Mt-CTAC $_{3.39}$. Each adsorbent was added at 2500 mg/L. The initial concentrations were 10 mg/L for MB, 30 mg/L for RB, and 10 parts per billion (ppb) for each PFAS. Subsamples were collected and analyzed for PFAS and dye concentrations at five time points: i.e., 0, 4, 8, 12, and 24 h. The modified Mt with the optimal CTAC/CEC ratio was selected and tested in the subsequent adsorption experiments.

The adsorption kinetics and isotherms of the optimal modified clay were assessed using mixtures consisting of the nine PFAAs, GenX, and two precursors (6:2 FTSA and N-EtFOSAA). Five concentration levels for each PFAS from the lowest level 1 to the highest level 5 were prepared in DI water without pH adjustment. The initial pH and concentration of each PFAS (C_0) at each level of the mixture were quantified at the beginning, as shown in Table 2. The dose of the tested adsorbent was 100 mg/L. Subsamples were collected at 1, 2, 4, 8, 12, and 24 h. Additionally, the adsorption performance of the unmodified and optimal modified clays was compared to that of three widely applied and commercially available adsorbents, i.e., FILTRA-SORB 400 GAC, a PAC (Calgon Carbon, Pittsburgh, PA, USA), as well as an adsorbent mainly consisting of AC, aluminum hydroxide, and kaolinite (AC/Al/clay-based). More experimental details are provided in Text S2 in the Supporting Information.

2.5. Data Analysis

The calculation of adsorbed PFAS per unit mass of an adsorbent and removal efficiencies (%) of compounds are detailed in Text S3 in the Supporting Information. The adsorption data of PFAS were evaluated by three widely applied kinetic models, i.e., pseudo-first-order (PFO), pseudo-second-order (PSO), and intraparticle diffusion (IPD) models, the equations of which are shown as

PFO:
$$q_t = q_e (1 - e^{-k_l t})$$
 (1)

PSO:
$$q_t = k_2 q_e^2 t / (1 + k_2 q_e t)$$
 (2)

IPD:
$$q_t = k_d t^{1/2} + C_d$$
 (3)

where t (h) is the contact time, q_t (mg/g) and q_e (mg/g) are the amounts of adsorbate in the solid phase at time t and equilibrium, respectively, k_1 (h⁻¹) and k_2 (g/(mg·h)) represent the rate constants for the pseudo-first- and pseudo-second-order reactions, respectively, $k_{\rm d}$ (mg/(g h^{1/2})) is the intraparticle diffusion coefficient, and $C_{\rm d}$ (mg/g) is the constant related to boundary layer thickness. The values of constants and coefficient can be generated from the slopes and intercepts of the linearized equations.

The adsorption data were fitted by three isotherm models, i.e., Langmuir, Freundlich, and Sips, given by eqs 4-6, respectively

Langmuir:
$$q_e = q_m K_L C_e / (1 + K_L C_e)$$
 (4)

Freundlich:
$$q_e = K_F C_e^{1/m}$$
 (5)

Sips:
$$q_e = q_m (K_S C_e)^{1/n} / (1 + (K_S C_e)^{1/n})$$
 (6)

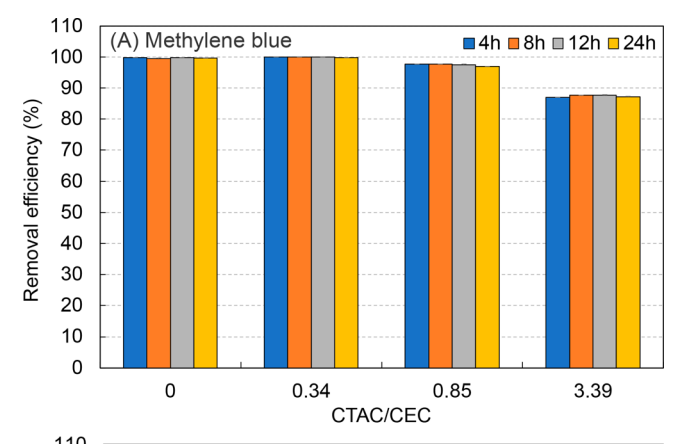
where $q_{\rm m}$ (mg/g) is the theoretical adsorption capacity, $C_{\rm e}$ (μ g/L; ppb) is the concentration of adsorbate in the aqueous phase at equilibrium, $K_{\rm L}$ (L/ μ g) is the Langmuir constant, $K_{\rm F}$ (mg L^{1/m}/(g μ g^{1/m})) is the Freundlich constant related to adsorption capacity and energy, m is the dimensionless heterogeneity coefficient indicating the favorability of the adsorption process, $K_{\rm S}$ (L/ μ g) is the Sips constant associated with adsorption affinity, and n is a dimensionless parameter qualitatively accounting for the heterogeneity of the adsorbate—adsorbent system.

3. RESULTS AND DISCUSSION

3.1. Adsorption Performance of Unmodified and Modified Clays with Coexposure to PFAS and Organic Dyes

The amount of surfactant loading in the modified clays may affect the distribution of surfactant cations/molecules within the Mt interlayer space and surfactant—Mt interactions, 44 thus leading to different adsorption performance. Three CTAC loadings were investigated, i.e., low, medium, and high CTAC/ CEC molar ratios of 0.34, 0.85, and 3.39, respectively, and an optimal ratio was expected to be selected based on the adsorption performance. To facilitate the screening process, we employed a coexposure adsorption method by mixing the cationic dye MB or the anionic dye RB with PFAS in the aqueous solution, since the dye colors can be easily monitored and serve as an indicator for adsorption performance.¹³ Moreover, with the presence of organic dyes, the adsorption performance of modified clays for organic pollutants and their effects on PFAS adsorption can be evaluated, which thus might broaden the applications of the modified clays. To quantify the concentrations of dyes simply by UV-visible spectroscopy, calibration curves between the concentrations and absorbances at 662 and 564 nm were developed for MB and RB, respectively, as shown in Figure S2. The initial concentrations of MB at 10 mg/L and RB at 30 mg/L fell in the linear ranges of the calibration curves.

The removal of MB and RB in the presence of PFAS by Na-Mt and the three modified clays, i.e., Mt-CTAC_{0.34}, Mt-CTAC_{0.85}, and Mt-CTAC_{3.39}, over contact times of 4, 8, 12, and 24 h, are shown in Figure 1. These results showed that the adsorption of MB by all four examined clays reached equilibrium within 4 h. The CTAC loading exhibited a negative effect on the adsorption of MB, with Na-Mt and Mt-CTAC_{0.34} showing the highest MB removal efficiency of nearly 100%, followed by Mt-CTAC_{0.85} and Mt-CTAC_{3.39} exhibiting approximately 97% and 87% removal efficiency, respectively. These findings are attributed to the fact that MB is a cationic dye (p K_a = 3.8), and the major mechanism of its adsorption by Na-Mt and Mt-CTAC_{0.34} is the cation exchange of MB⁺ with $\mathrm{Na}^{+}.^{45}$ For Mt-CTAC_{0.85} and Mt-CTAC_{3.39}, in which Na^{+} had been largely or fully exchanged, hydrophobic interactions mainly contributed to adsorption of the hydrophobic MB.⁴⁵ In contrast, CTAC/CEC ratios affected RB adsorption positively in the range of 0-0.85, showing that Mt-CTAC_{0.85} adsorbed nearly 100% of RB within 4 h while Na-Mt had almost no adsorption. The positive effect of CTAC loadings, however,



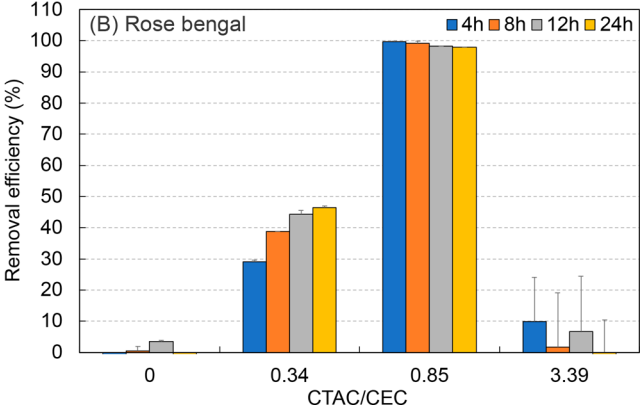


Figure 1. Adsorption (removal efficiency) of methylene blue (A) and rose bengal (B) by the unmodified (Na-Mt) and three modified clays (Mt-CTAC_{0.34}, Mt-CTAC_{0.85}, and Mt-CTAC_{3.39}) with the coexistence of PFAS. The initial concentrations of each PFAS, MB, and RB were 10 ppb, 10 mg/L, and 30 mg/L, respectively. Error bars represent the standard deviations of triplicate measurements.

was not applicable to Mt-CTAC_{3.39}, which adsorbed RB weakly with a removal efficiency of <10%. The extremely low adsorption of RB by Na-Mt might be due to electrostatic repulsion between the negatively charged clay surface and RB molecules. With increasing CTAC loading, hydrophobic interactions start to play a role in adsorption of the hydrophobic RB.⁴⁶ However, the large molecular dimensions of RB with benzene and xanthene moieties (Figure S1B), as well as the severe blocking of the Mt interlamellar space caused by the large intercalated CTA⁺ cations at a CTAC/CEC loading of 3.39,³⁰ might inhibit the intrusion of RB molecules into the interlayer space of Mt.

PFAS adsorption on the four clays in the presence of MB or RB was also evaluated (Figure 2). The results showed that CTAC loadings had a positive effect on PFAS adsorption, with Mt-CTAC $_{0.85}$ and Mt-CTAC $_{3.39}$ adsorbing nearly 100% of PFAS and Na-Mt showing extremely low adsorption. Specifically, Mt-CTAC $_{0.85}$ displayed the best adsorption performance among the four clays, removing 100% of almost all PFAS in the presence of either MB or RB. The adsorption reached equilibrium within 4 h, and no desorption was observed during longer contact times. Interestingly, although the examined PFAS were also anionic because of the low p K_a (Table 1), Mt-CTAC $_{3.39}$ exhibited a adsorption capacity comparable with that of Mt-CTAC $_{0.85}$ for almost all PFAS, in contrast to the low adsorption observed for RB. This might be due to the linear structures and smaller molecular

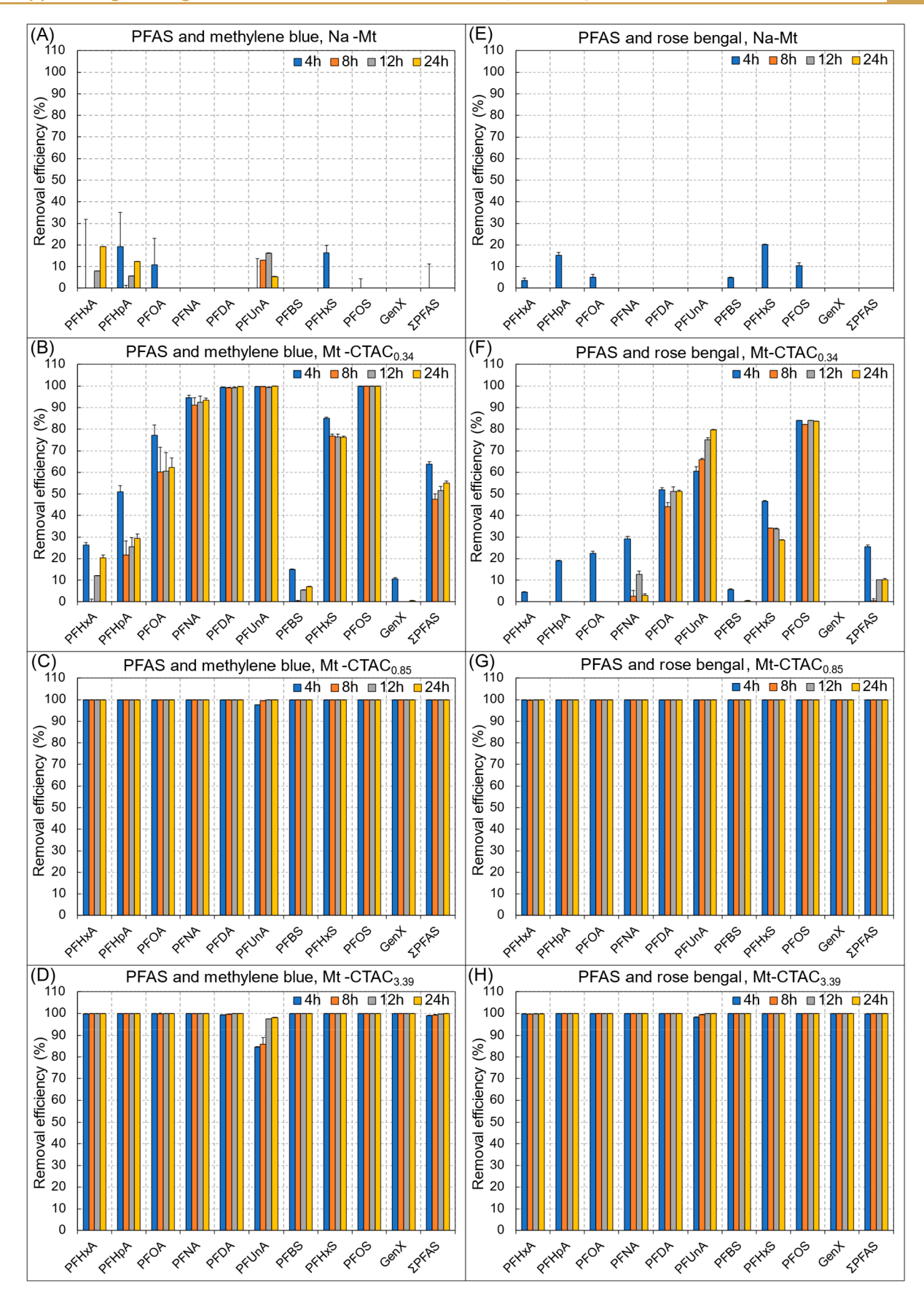


Figure 2. Adsorption of PFAS by the unmodified (Na-Mt) and three modified (Mt-CTAC_{0.34}, Mt-CTAC_{0.85}, and Mt-CTAC_{3.39}) clays with coexposure of the organic dye (methylene blue or rose bengal). The initial concentrations of each PFAS, MB, and RB were 10 ppb, 10 mg/L, and 30 mg/L, respectively. Error bars represent the standard deviations of triplicate measurements.

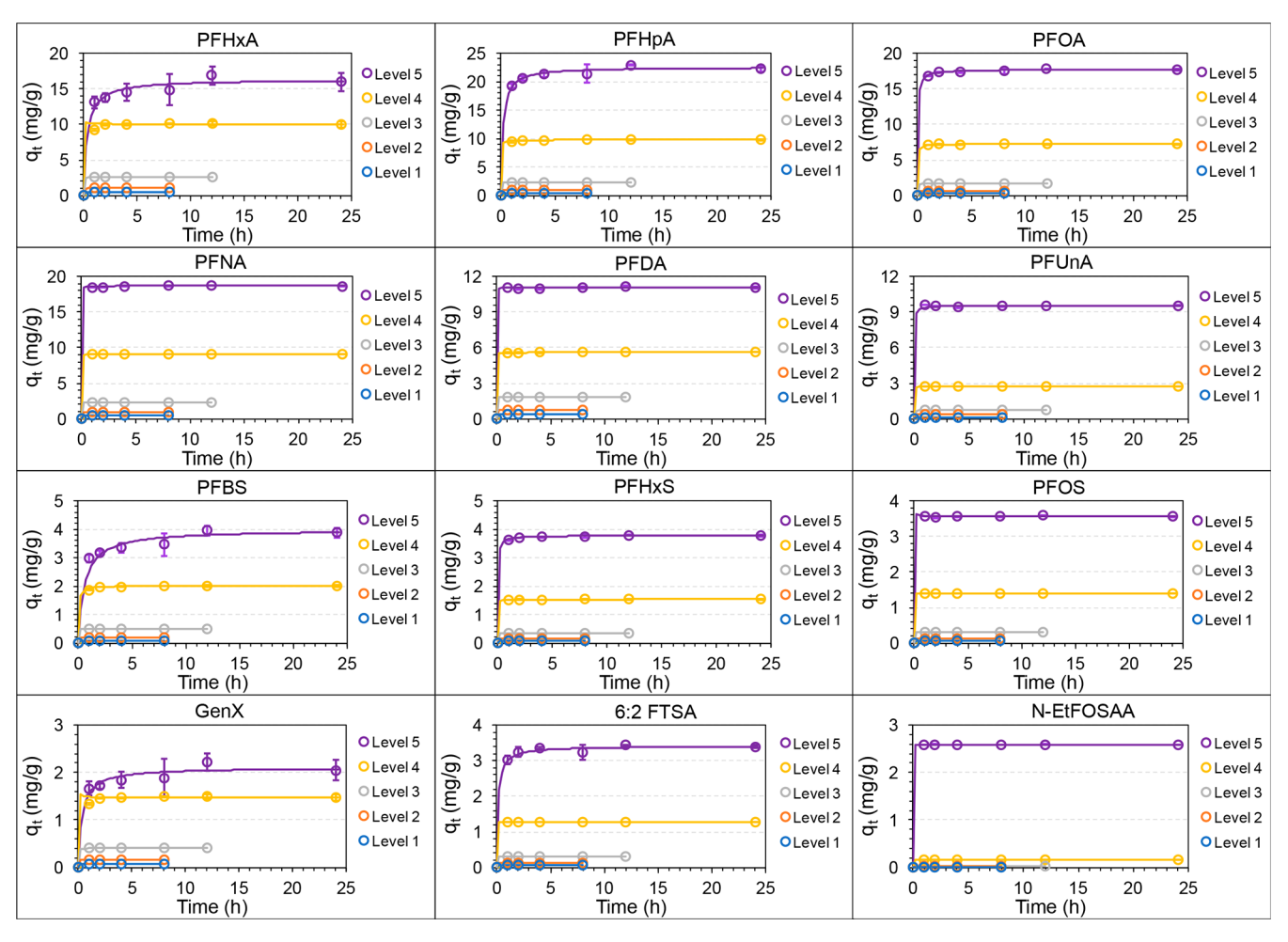


Figure 3. Kinetics of adsorption of PFAS at different initial concentration levels by Mt-CTAC $_{0.85}$. The colored circle points indicate experimental data at each initial concentration level. The colored solid lines indicate fitting lines of the pseudo-second-order model for experimental data points with the same colors. Error bars represent the standard deviations of triplicate measurements.

dimensions of PFAS than of RB, which facilitated the entering of PFAS into the Mt interlayer space. Similarly to RB, negligible PFAS were adsorbed by Na-Mt, probably due to the electrostatic repulsion. In comparison, the amounts of adsorbed PFAS by Mt-CTAC_{0.34} were dependent on carbon chain length with higher PFAS adsorption for longer-chain PFCAs and PFSAs. The increasing adsorption of PFAS with longer chain length indicated that hydrophobic interactions may play a critical role in the adsorption. Moreover, PFSAs were more easily adsorbed by Mt-CTAC_{0.34} than PFCAs with the same chain length, which might be attributed to the lower water solubility (Table 1) and thus higher hydrophobicity of the former than the latter. This also highlights the important role of hydrophobic interactions between PFAS carbon chains and CTA+ alkyl chains in the PFAS adsorption process. It can also be observed that MB, compared to RB, seemed to lead to enhanced adsorption of PFAS, which might be due to electrostatic attractions between cationic MB and anionic PFAS. From the findings related to the adsorption of organic dyes and PFAS, Mt-CTAC_{0.85} was chosen as the optimal modified clay and evaluated further in this study.

3.2. Adsorption Kinetics of PFAS by the Optimal Modified Clay

The selected optimal modified clay, Mt-CTAC $_{0.85}$, was exposed to aqueous mixtures of 12 PFAS with a series of 5 initial

concentration levels. To evaluate the adsorption performance of Mt-CTAC $_{0.85}$ and to comparatively investigate the adsorption kinetics of different PFAS, three kinetic models—PFO, PSO, and IPD—were applied to fit the adsorption data. The fitting correlations were evaluated using the linear forms of the models. As displayed in Figures S3 and S4, the squared correlation coefficients R^2 for all 12 PFAS fitted by the linearized PFO and IPD models were quite low, ranging from 0.317 to 0.734 and from 0.358 to 0.594, respectively. In contrast, the linearized PSO model showed excellent fitting correlations, with R^2 values of 0.996–1 for the 12 PFAS (Figure S5), indicating that the adsorption kinetics of all examined PFAS are well described by the PSO model. Thus, we applied the PSO model to fit all the adsorption kinetic data of the 12 PFAS, as shown in Figure 3.

It can be seen from the results that a fast adsorption process occurs within the first 1 h of contact time (Figure 3). At the lower initial concentrations of levels 1-3, adsorption reached a maximum within 1 h for all PFAS, and all removal efficiencies were 100% (Figure 4), indicative of the expeditious kinetics and high adsorption capacity of Mt-CTAC_{0.85}. Regarding the higher initial concentrations of levels 4 and 5, an adsorption manner dependent on carbon chain length was observed, with higher removal efficiency for PFAS with the longer chain length, which is consistent with the findings in section 3.1. In detail, at the initial concentration of level 4, for long-chain

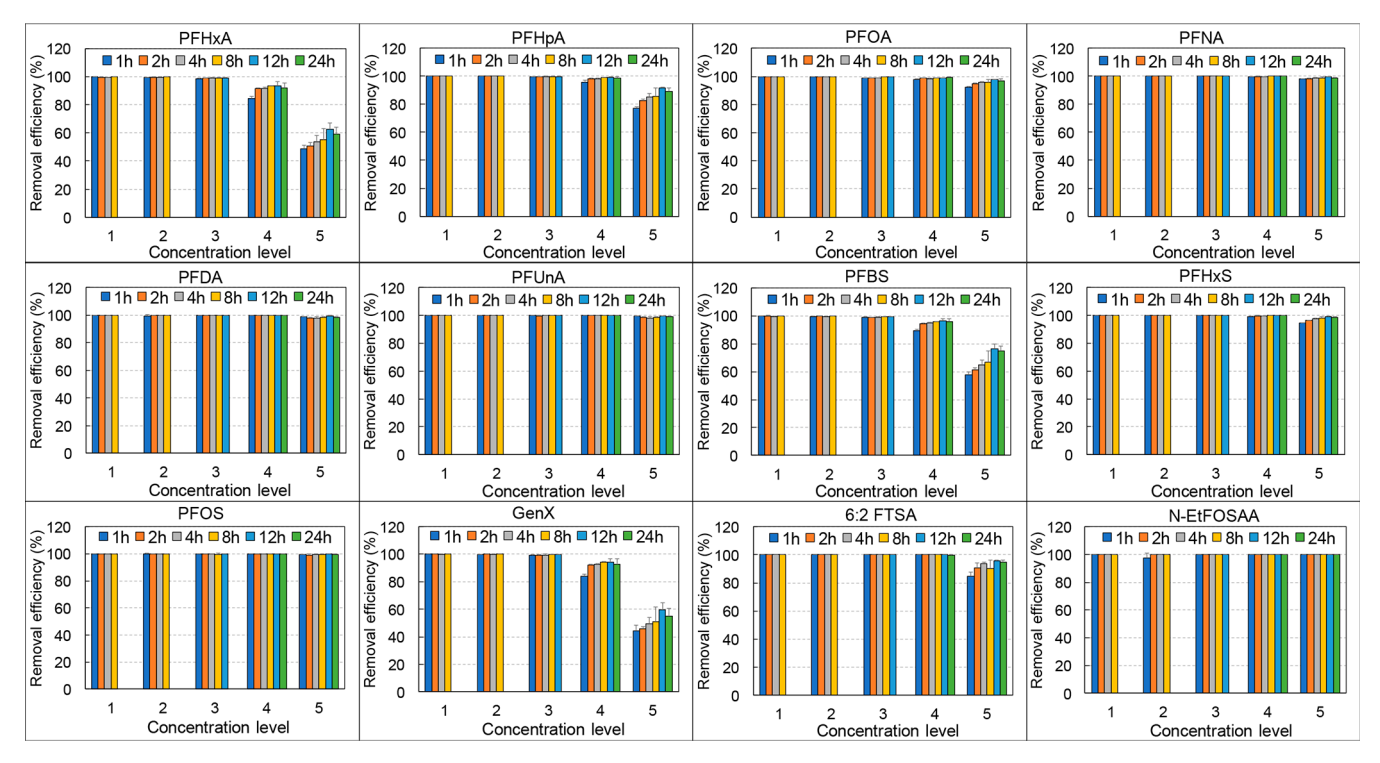


Figure 4. Removal efficiency of PFAS at different initial concentration levels and different contact times (1, 2, 4, 8, 12, and 24 h) for Mt-CTAC_{0.85}. Error bars represent the standard deviations of triplicate measurements.

PFCAs and PFSAs (i.e., PFOA, PFNA, PFDA, PFUnA, PFHxS, and PFHxS), as well as the two long-chain precursors (i.e., 6:2 FTSA and N-EtFOSAA), saturated adsorption with 100% removal efficiency was achieved within 1 h and no desorption was detected. However, within the same contact time, short-chain PFCAs and PFSAs (i.e., PFHxA, PFHpA, and PFBS), as well as GenX, were not fully adsorbed, with removal efficiencies ranging from 84% to 96%. For these PFAS, the adsorption process continued to occur with increasing contact time and reached equilibrium within 2 h. Consequently, the whole adsorption process can be divided into three phases. In the first phase, PFAS are mainly adsorbed into the interlayers of the modified clay. In the second phase, the electrostatic repulsion between PFAS anions slows continued PFAS adsorption. Equilibrium is reached in the third phase. This multiple-phase adsorption process was similarly observed in the adsorption of 4-nitrophenol by the modified clay.³⁰ At the initial concentration of level 5, similar adsorption behavior with three phases was observed for short-chain PFAS, but with lower removal efficiency and a longer second phase than those at level 4. PFOA, PFHxS, and 6:2 FTSA, which possess shorter chain lengths compared to other long-chain PFAS, also exhibited unsaturated adsorption within 1 h. Thus, as shown in Figure S6, the PFAS chain length and concentration significantly affected the performance of the adsorbent.

3.3. Adsorption Isotherms of PFAS by the Optimal Modified Clay

Due to the excellent adsorption capacity of Mt-CTAC_{0.85}, the PFAS concentrations in the aqueous phase were either close to or lower than the limit of detection (LOD) in the case of lower concentration levels and long-chain PFAS. Therefore, it was not feasible to obtain $C_{\rm e}$ values for fitting isotherm models for individual compounds. Moreover, a similar adsorption mechanism might be shared by all the examined PFAS due

to their comparable and shared physicochemical properties. Thus, the total $q_{\rm e}$ and $C_{\rm e}$ values of all PFAS tested in this study were calculated and employed to establish isotherm models. Three common isotherm models, namely Langmuir, Freundlich, and Sips, were used to fit experimental adsorption data. The Langmuir isotherm considers the dynamic equilibrium of adsorption and desorption, while the Freundlich isotherm predicts adsorption processes occurring on heterogeneous surfaces. In comparison, the Sips model combines the Langmuir and Freundlich isotherms, aiming to predict adsorption in heterogeneous systems. 47

As evidenced in Figure 5, the Langmuir model fit the experimental adsorption data very well in the high-concentration range and the Freundlich isotherm exhibited excellent fits in the low range, while the Sips isotherm satisfactorily fit the whole range of data (Table 3). The Sips isotherm has been shown to overcome the limitations of the increasing adsorbate concentration related to the Freundlich model.⁴⁸ It is essentially a Freundlich model at low adsorbate concentrations and predicts the monolayer adsorption similarly to the Langmuir model at high adsorbate concentrations. It was reported that there was a preference for the formation of a monolayer on the aqueous clay surface for PFAS molecules at high concentrations. 49 The adsorption of PFOS and PFOA onto ferrihydrite⁵⁰ and PFOS onto goethite also exhibited monolayer formation.⁵¹ As shown in Table S3, at low concentrations, the q_e values determined by the Sips isotherm were closer to those predicted by the Freundlich isotherm, while at high concentrations, the q_e values predicted by the Sips model were closer to those generated from the Langmuir model, indicating the successful application of the Sips isotherm to model the adsorption process. The adsorption capacity of Mt-CTAC_{0.85} was predicted by the Sips model to be 255.27 mg/g (Table 3).

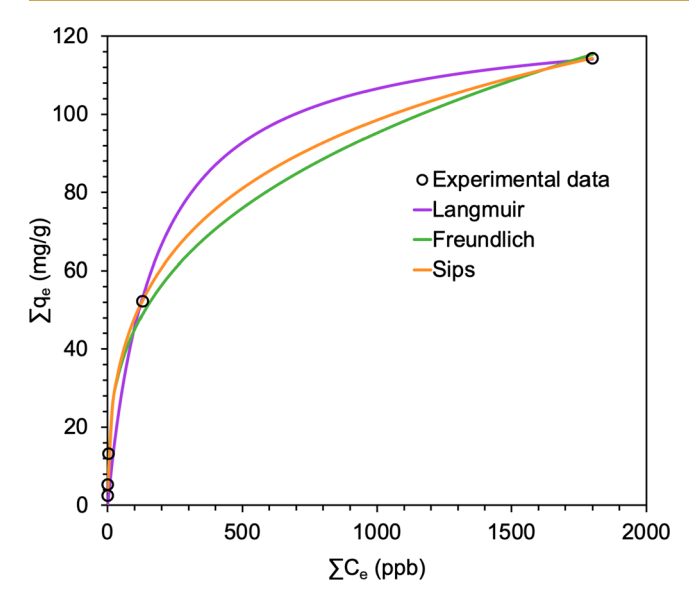


Figure 5. Adsorption isotherms of total PFAS for Mt-CTAC $_{0.85}$, plotted with the Langmuir, Freundlich, and Sips models. Experimental data represent the mean values of triplicate measurements.

Table 3. Parameters and Values Derived from Adsorption Isotherm Models of Langmuir, Freundlich, and Sips in the Adsorption Process of Mt-CTAC_{0.85}

model	parameter	value
Langmuir	R^2	0.9850
	$K_{ m L}~({ m L}/\mu{ m g})$	5.709×10^{-3}
	$q_{ m m}~({ m mg/g})$	125.22
Freundlich	R^2	0.9966
	$K_{\mathrm{F}} \left(\mathrm{mg} \ \mathrm{L}^{1/m} / (\mathrm{g} \cdot \mu \mathrm{g}^{1/\mathrm{m}}) \right)$	10.028
	m	3.070
Sips	R^2	0.9998
	$K_{ m S}~({ m L}/\mu{ m g})$	3.427×10^{-4}
	$q_{ m m}({ m mg/g})$	255.27
	n	2.302

3.4. Comparison of Adsorption Performance between the Optimal Modified Clay and Commercial Adsorbents

The modified clay Mt-CTAC $_{0.85}$ and unmodified Na-Mt were compared in parallel with three commercially available adsorbents that are widely used in practice. The commercial adsorbents were FILTRASORB 400 GAC and a PAC product from Calgon Carbon, as well as an AC/Al/clay-based adsorbent. Due to confidentiality, the name of the third ACbased composite adsorbent cannot be disclosed here. As shown in Figure 6, compared to the three commercial adsorbents, the unmodified Na-Mt exhibited the lowest removal efficiency overall, while the modified clay Mt-CTAC_{0.85} demonstrated the highest removal of the 13 PFAS, including 3 precursors. PAC exhibited the second-best adsorption performance among the five adsorbents. As evidenced by the adsorption kinetic results and those in Figure 6 and previous research, 52 the removal of PFAS by Mt-CTAC_{0.85} was significantly faster and higher than those by PAC. Within 4 h, the concentrations of all PFAS approached zero in the tested systems for Mt-CTAC_{0.85}. For those with PAC, however, PFAS at the low end of ppt were still detectable. Additionally, the modified clay was highly efficient for adsorbing one PFAS precursor, 8:2 diPAP, for which PAC was not highly effective. The GAC and the AC/Al/clay-based adsorbent showed quite similar removal profiles for all PFAS, with notably low removal at $t=4\,\mathrm{h}$ and gradually increasing removal with longer contact times, indicating the slow adsorption kinetics for both adsorbents.

A commercial adsorbent, FLUORO-SORB, a patented modified clay, has been shown to have high efficiency in removing PFAS in contaminated groundwater. 47 Batch adsorption experiments were carried out with various adsorbents, including FLUORO-SORB 200, ion-exchange resin, GAC (reagglomerated bituminous type), and hardwood-based biochar. The adsorbent dose was 12.5, 50, or 100 mg/L with an adsorption time of 168 h (7 days). The adsorption of 10 PFAAs and 5 precursors by FLUORO-SORB 200 was rapid in the initial 12 h and then slowed until equilibrium was reached within 168 h.⁴⁷ Our modified clay showed that, at t = 48 h, all PFAS in the liquid phase were undetectable except PFHxA with a final concentration of less than 100 ppt. For FILTRASORB 200, most PFAS in the aqueous phase at t = 48 h were still at a relatively high levels.⁴⁷ For example, at 48 h both PFOA and PFOS were at a level of \sim 2 ppb with initial concentrations of 6 and 15 ppb, respectively. It is worth noting that the adsorption performance of the adsorbent in real groundwater may be affected by various environmental factors, which needs to be considered in future investigations on their more comprehensive compar-

The modified clay Mt-CTAC_{0.85} also exhibited an adsorption capacity superior or comparable to those in literature data of conventional or emerging adsorbents (Table 4). For instance, Zhi and Liu⁵³ investigated the same FILTRASORB 400 GAC as we did and Calgon Carbon's BPL PAC, both of which showed an adsorption capacity of around 2.5 mg/g for both PFOA and PFOS (Table 4), much lower than those of our modified clay with coexposure to a PFAS mixture. A commercial clay-based adsorbent, matCARE, displayed a 50 mg PFOS/g adsorption capacity with high adsorbent dose and initial PFOS concentrations (Table 4). Additionally, in comparison with documented data of other modified clays in lab-scale tests (Table 4), Mt-CTAC_{0.85} showed a comparable adsorption performance for total PFAS.

The comparison of adsorbent adsorption performance, however, is relative. The adsorption performance can be affected by numerous factors: for example the target PFAS and their concentrations, solution pH and ionic strength, adsorbent dose and structure, etc. As shown in Table 4, almost all reported adsorption studies focused on either PFOA or PFOS or both. Since these two long-chain PFAS can be removed well by most adsorbents, including our modified clay, the adsorption capacity of the adsorbents in Table 4 theoretically should have lower capacity for short-chain PFAS. In this study, the use of a mixed PFAS including PFAAs, GenX, and precursors considered the fact that PFAS in most contaminated environments exist in mixtures. Environments contaminated by an industrial process that only uses a specific PFAS may be an exception. As competition between different PFAS during adsorption is likely, this competition might be revealed by comparing the adsorption behavior of an adsorbent exposed to one or two PFAS. However, given the large number of combinations to be tested for this purpose, we chose to test a mixture representing different types of PFAS. This time-saving approach allowed us to narrow down the list of adsorbents and

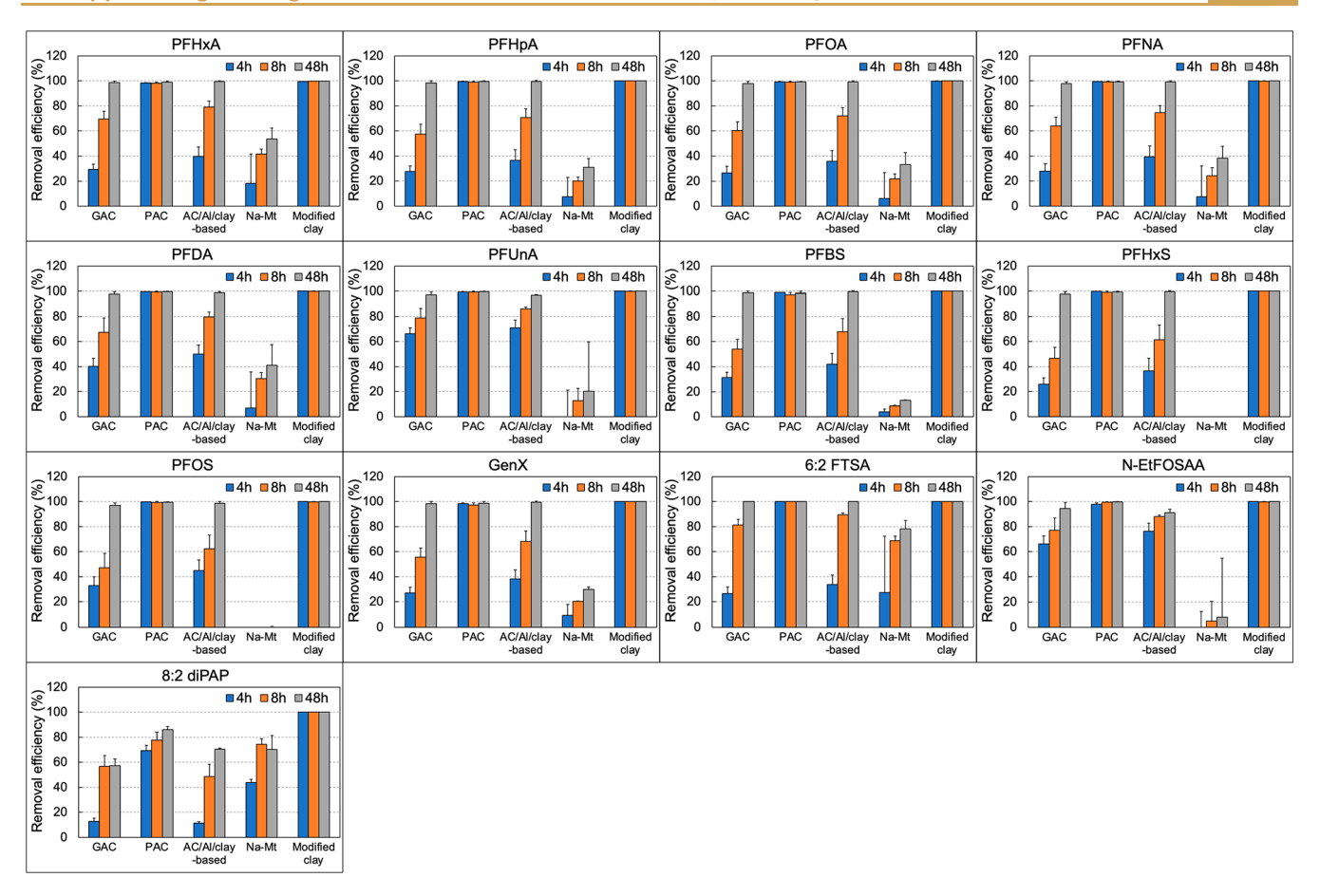


Figure 6. Adsorption performance comparison among Na-Mt, Mt-CTAC_{0.85}, and commercially available FILTRASORB 400 GAC, PAC, and an AC/Al/clay-based adsorbent for a PFAS mixture at different contact times (4, 8, and 48 h). The initial concentration of each PFAS in the mixture was 10 ppb. Error bars represent the standard deviations of triplicate measurements.

ī

Table 4. Adsorption Performance of Carbon- and Clay-Based Adsorbents in the Literature

adsorbent	dosage (mg/L)	PFAS	$\binom{C_0}{(\mathrm{ppm})}$	capacity (mg/g)
FILTRASORB 400 GAC ⁵³	200	PFOA	0.5	2.52
		PFOS	0.5	2.59
BPL PAC ⁵³	200	PFOA	0.5	2.49
		PFOS	0.5	2.48
matCARE ⁵⁴	10000	PFOS	215	50
modified clay ³¹	50	PFOA	5	207 ^a
		PFOS	5	403 ^a
modified clay ¹⁷	N/A	PFOA	95	~62 ^b
		PFOS	124	~339 ^b

^aThe highest values obtained by isotherm models. ^bEstimation from the figure in the reference for the modified clay with a HDTMAB/CEC ratio of 0.5. The mass of PFAS was calculated using the molecular weight in Table 1.

gave us time and resources to engage in detailed studies of the best-performing adsorbents.

3.5. Adsorption Mechanism Interpretation with Insights from Physicochemical Characterizations

A physicochemical characterization of Na-Mt and Mt-CTAC_{0.85} was conducted to examine their differences and to better understand the adsorption mechanisms of the modified clay. As shown in SEM images (Figure 7A,B), both Na-Mt and

Mt-CTAC_{0.85} displayed large agglomerated particles with irregular shapes, which were formed by numerous tiny particles. The void spaces of interparticle cavities among those small particles led to the macroporous structures of the larger aggregated clay particles, which could play a significant role in PFAS adsorption by facilitating diffusion of the adsorbate through cavities.⁵⁵ Na-Mt presented a coarse and rough surface containing many interparticle cavities, while Mt-CTAC_{0.85} exhibited a smoother surface resulting from the modification process. An EDS analysis (Figure 7C,D) of Na-Mt indicated that O, Si, Al, and Fe were the major elements, accounting for >90% of the total elemental compositions, which is consistent with previous findings related to the structural formula of Mt. ^{47,56} After modification, the contents of the major elements showed slight variations because of the replacement of Na+ by CTA+ cations, which resulted in a significant decrease of Na content in Mt-CTAC_{0.85}. It is worth noting that electrically conductive carbon tapes were applied in the preparation of SEM-EDS samples, and therefore the element C was not included in the EDS measurement and analysis. This might result in elemental compositions varying from the true values that can be obtained by more accurate elemental analysis methods, such as inductively coupled plasma optical emission spectroscopy (ICP-OES).

The specific surface area and pore volume of Mt-CTAC $_{0.85}$ compared to those of Na-Mt were evaluated by a BET measurement. To obtain the original values, the samples were first activated at room temperature, at which the adsorbents are

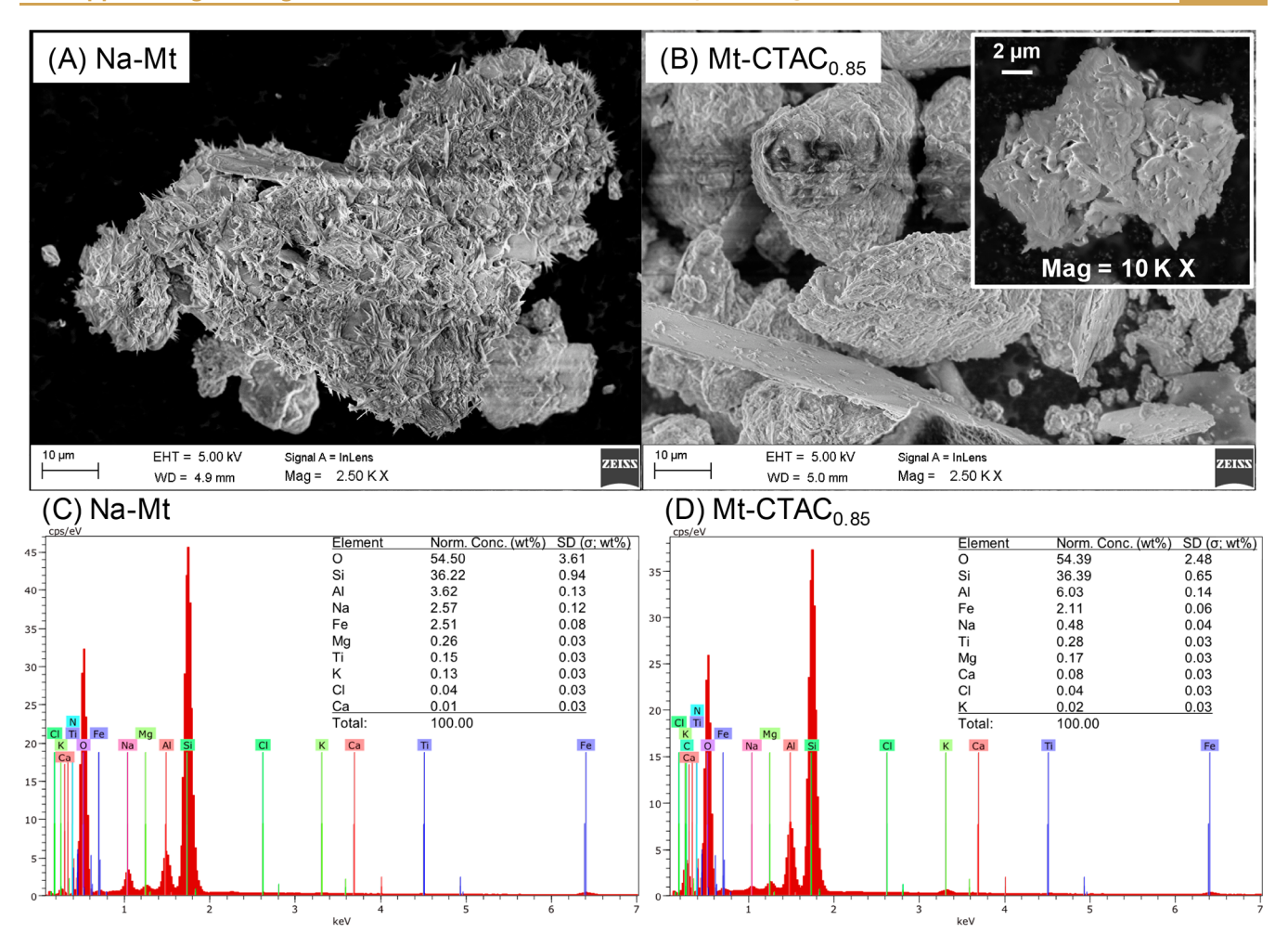


Figure 7. Morphological (A, B) and compositional (C, D) analyses of Na-Mt (A, C) and Mt-CTAC $_{0.85}$ (B, D) by SEM-EDS. Elemental compositions are shown with normalized concentrations (wt %) and standard deviations (SD). The elements not shown were undetectable, which were lower than the detection limit of 0.01 wt %.

normally used in practice. As shown in Figure 8A, Mt-CTAC_{0.85} possessed a BET surface area of 10.58 m²/g and a pore volume of 0.0145 cm³/g, 30% and 20% lower than those of Na-Mt, respectively. This finding may be attributed to the clogging of interlayer spaces by the CTAC molecules after modification. After activation at 100 and 200 °C, the pore volume of Na-Mt rose, presumably due to the removal of adsorbed species at these higher temperatures. Regarding Mt-CTAC_{0.85}, the surface area and pore volume were slightly elevated after activation at 100 °C and increased dramatically to 45.34 m²/g and 0.0317 cm³/g, respectively, after activation at 200 °C. Previous findings suggested that the chemical structures of quaternary ammonium cations in the modified clay could affect the basal spacing of the clay backbone, ⁴⁷ since the surfactant molecules might enlarge the interlayer spaces. After activation at high temperature for a long time, these surfactants may evaporate from the material, leaving behind expanded interlayer void space detectable by gas adsorption measurements. These findings give valuable insights into the potential regeneration of spent modified clays.

To further interpret the adsorption mechanism of the modified clay, a critical parameter influencing the adsorption process, the ζ potential, was determined and analyzed. In general, Mt-CTAC_{0.85} exhibited a positive charge while Na-Mt had a negative charge over the wide range of pH values tested

(Figure 8B). The original pH and ζ potential without any adjustments of Mt-CTAC_{0.85} were 7.46 and 46 mV, respectively, in contrast with 11.38 and -31.6 mV, respectively, for Na-Mt. The pH_{PZC} value was 10.05 for Mt-CTAC_{0.85} and 0.34 for Na-Mt. Such a neutral original pH and high pH_{PZC} of Mt-CTAC_{0.85} are favorable for its application in the environmental matrices, in which PFAS are typically negatively charged. Prior studies have also demonstrated that more positively charged adsorbents possessed a higher tendency to adsorb PFAS. 40,57

The effect of clay modification on PFAS adsorption was further investigated by FTIR through the comparative examination of Na-Mt, pristine Mt-CTAC_{0.85}, and two spent Mt-CTAC_{0.85} adsorbed PFAS mixtures at levels 4 and 5. As displayed in Figure 8C, the FTIR spectra of all samples exhibited bands at 3697 and 3620 cm⁻¹, which were attributed to the O–H stretching vibration of the structural hydroxyl groups of the clay. ^{58,59} All four samples also displayed an intense band at ca. 1000 cm⁻¹ corresponding to the Si–O–Si stretching and a band at 692 cm⁻¹ matching the bending mode of the same group. ^{59,60} Similarly, the bands at 912 and 798 cm⁻¹, which were ascribed to Al–OH–Al bending and Si–O symmetric stretching, respectively, ^{59,61} were also present for all samples. All spectra also presented the typical O–H bending at 1636 cm⁻¹ due to the residue of adsorbed water. ^{62,63} These

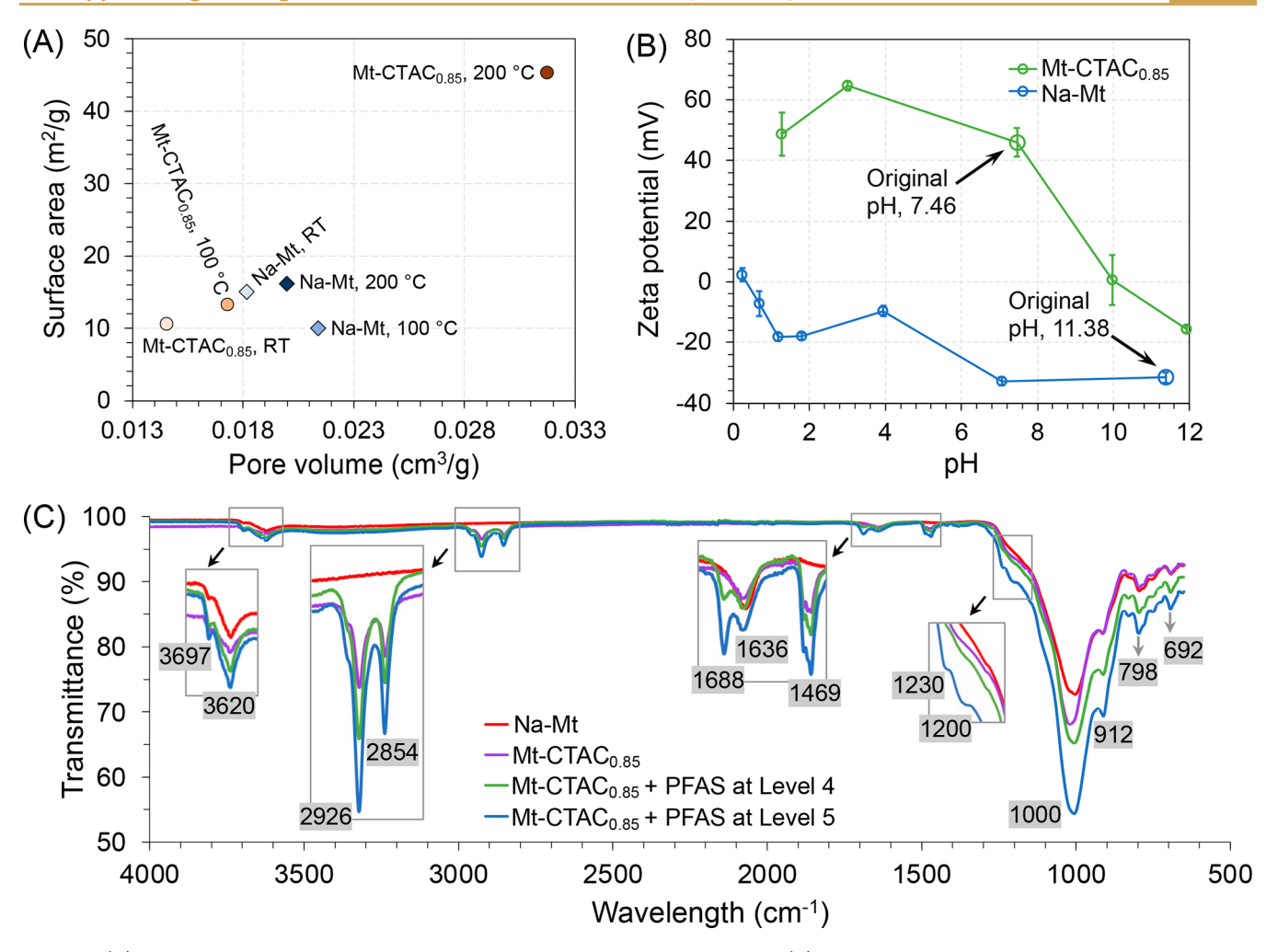


Figure 8. (A) Surface area and pore volume of Na-Mt and Mt-CTAC $_{0.85}$ analyzed by BET. (B) Relationship between ζ potential and pH for Na-Mt and Mt-CTAC $_{0.85}$. (C) FTIR spectra of Na-Mt, pristine Mt-CTAC $_{0.85}$, and spent Mt-CTAC $_{0.85}$ after exposure to PFAS mixtures at levels 4 and 5. Error bars represent the standard deviations of triplicate measurements.

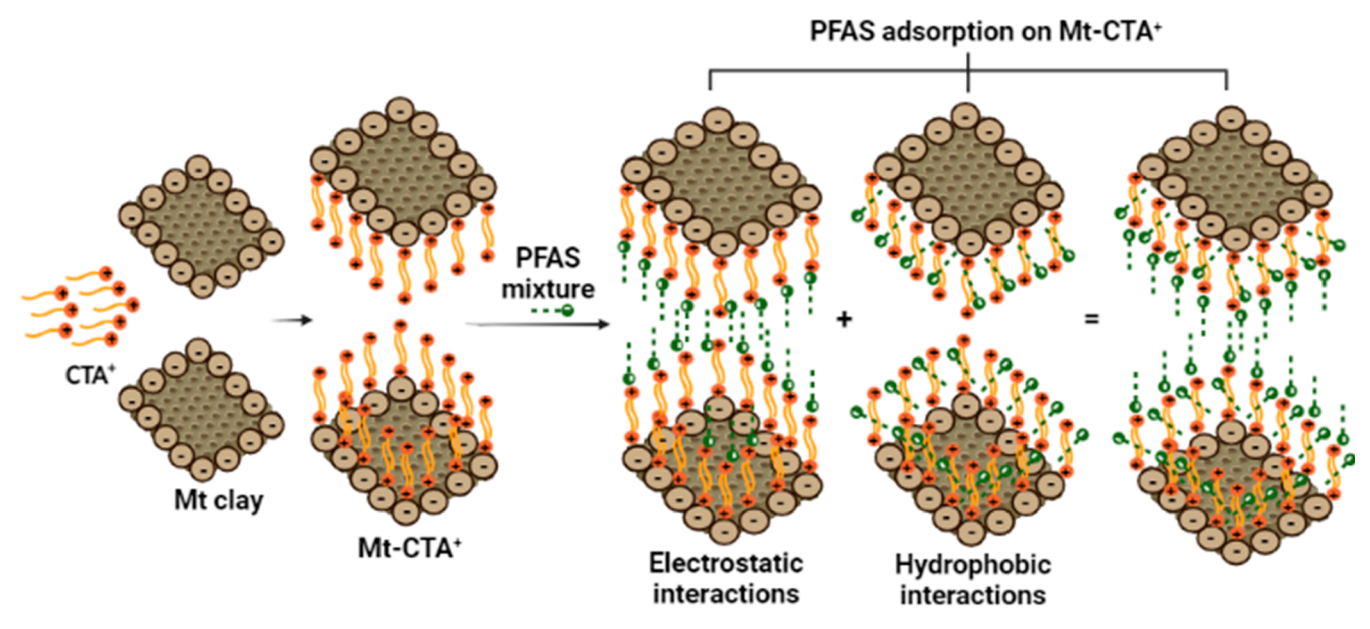


Figure 9. Proposed mechanisms for the CTAC modification process and adsorption of PFAS on the modified clay.

observations, combined with the above SEM-EDS results, suggested that CTAC modification and PFAS adsorption

exerted a limited effect on the clay backbone structure. The modification seemed to only affect the surface, while the main

structure and the relative content of each element of the clay backbone remained similar. This was also verified by XRD, showing indistinguishable crystal structures between Na-Mt and Mt-CTAC $_{0.85}$ (Figure S7). Similar findings were also observed for matCARE 54 and in previous literature.

Interestingly, only the pristine and spent Mt-CTAC_{0.85} samples exhibited bands at 2926, 2854, and 1469 cm⁻¹. The bands at 2926 and 2854 cm⁻¹ were attributed to the asymmetric and symmetric stretching vibrations of C-C in the alkyl chain, respectively,⁵⁹ while the band at 1469 cm⁻¹ corresponded to the C-H bending in the same chain. 65 This indicated the presence of CTAC in the pristine and spent modified clays. Moreover, a band at 1688 cm⁻¹, which was ascribed to the C=O stretching, 66,67 was only exhibited in the spectra of the two spent modified clays, while it was absent in the spectra of Na-Mt and pristine Mt-CTAC $_{0.85}$. The weak bands at 1230 and 1200 cm $^{-1}$ appearing in the spectra of spent Mt-CTAC_{0.85} with exposure to PFAS at level 5 matched up with CF₂ and CF₃ groups.⁶⁸ These findings demonstrated the adsorption of PFAS on the spent modified clays. The characteristic band of the sulfonic groups (1048 cm⁻¹) was not found in the spectra of the spent Mt-CTAC_{0.85}, probably due to the relatively lower amounts of PFSAs than PFCAs in the mixtures and the overlapping effect of the broad and strong Si-O-Si stretching band.

In summary, considering all of the findings above, we proposed an adsorption mechanism of PFAS to Mt-CTAC $_{0.85}$ involving electrostatic interactions between the positively charged CTA+ cations and the negatively charged PFAS anions, as well as hydrophobic interactions between PFAS carbon chains and CTA+ alkyl chains (Figure 9). It has been demonstrated that the Langmuir isotherm is greatly affected by electrostatic interactions⁷⁰ and that the Freundlich isotherm is strongly associated with hydrophobic interactions. 54 The better fitting of our adsorption isotherm data to Langmuir and Freundlich isotherms at high and low concentrations, respectively, supported this proposition that electrostatic interactions were dominant at a high concentration and that hydrophobic interactions became increasingly governing as the concentration decreased. A prior study combining experimental and molecular simulation also indicated that multiple interactions accounted for PFAS adsorption on modified clay. 47 Further investigations, both experimental and modeling, are necessary to verify the proposed PFAS adsorption mechanism. The verified mechanism will be beneficial for redesigning and synthesizing better adsorbents for PFAS removal. While it is beyond the scope of this study, future research should also be devoted to the regeneration, as well as the effects of environmental factors, such as pH, ionic strength, and natural organic matter, on the adsorption performance of the modified clay for its practical application in a real aqueous environment.

4. CONCLUSIONS

Our CTAC-modified clays with medium and high CTAC/CEC ratios exhibited remarkably enhanced capabilities to adsorb PFAS mixtures compared to the unmodified clay. The optimal modified clay with the medium CTAC/CEC ratio, Mt-CTAC $_{0.85}$, displayed fast adsorption kinetics that were perfectly fitted by the PSO model. The adsorption behavior was significantly dependent on the initial concentration and carbon chain length of PFAS. The Sips isotherm model precisely predicted the adsorption process of the total PFAS with a

calculated adsorption capacity of 255.27 mg/g for Mt-CTAC $_{0.85}$. In comparison with other commercial adsorbents, Mt-CTAC $_{0.85}$ showed superior adsorption performance for all PFAS, including precursors. A comparative physicochemical characterization of the clays studied herein facilitated an interpretation of the excellent adsorption performance of Mt-CTAC $_{0.85}$ and elucidation of the mechanism by which it adsorbs PFAS. In light of all findings in this study, an adsorption mechanism associated with electrostatic interactions and hydrophobic interactions was proposed.

ASSOCIATED CONTENT

Supporting Information

The Supporting Information is available free of charge at https://pubs.acs.org/doi/10.1021/acsaenm.2c00096.

Experimental details and additional adsorption, kinetic, isotherm, and characterization data (PDF)

AUTHOR INFORMATION

Corresponding Author

Tao Jiang — Department of Environmental and Sustainable Engineering, University at Albany, State University of New York, Albany, New York 12222, United States; Present Address: 1400 Washington Avenue, Albany, NY 12222, USA; ⊚ orcid.org/0000-0003-1582-9885;

Email: tjiang2@albany.edu

Authors

Weilan Zhang — Department of Environmental and Sustainable Engineering, University at Albany, State University of New York, Albany, New York 12222, United States; orcid.org/0000-0003-3148-1751

Aswin Kumar Ilango – Department of Environmental and Sustainable Engineering, University at Albany, State University of New York, Albany, New York 12222, United States

Jeremy I. Feldblyum – Department of Chemistry, University at Albany, State University of New York, Albany, New York 12222, United States; orcid.org/0000-0001-6667-9587

Zheng Wei — Department of Chemistry, University at Albany, State University of New York, Albany, New York 12222, United States

Haralabos Efstathiadis — College of Nanoscale Science and Engineering, SUNY Polytechnic Institute, Albany, New York 12203, United States

Mehmet V. Yigit — Department of Chemistry and The RNA Institute, University at Albany, State University of New York, Albany, New York 12222, United States; ● orcid.org/0000-0002-4349-3701

Yanna Liang — Department of Environmental and Sustainable Engineering, University at Albany, State University of New York, Albany, New York 12222, United States; orcid.org/0000-0003-1720-1039

Complete contact information is available at: https://pubs.acs.org/10.1021/acsaenm.2c00096

Notes

The authors declare no competing financial interest.

L

ACKNOWLEDGMENTS

The authors acknowledge financial support from the University at Albany (UAlbany), State University of New York, funding from the U.S. National Science Foundation under award number CBET 2225596, and support from the donors of the American Chemical Society Petroleum Research Fund under award number 59835-DNI10. We appreciate Calgon Carbon for providing FILTRASORB® 400 GAC and PAC adsorbents and an anonymous company for providing the AC-based adsorbent. We are also grateful to Kevin Shah from SUNY Polytechnic Institute for his assistance with SEM-EDS measurements, to Tianran Zhai from UAlbany for BET analyses, and to Mahera Kachwala from UAlbany for help with ζ potential quantifications.

REFERENCES

- (1) Buck, R. C.; Franklin, J.; Berger, U.; Conder, J. M.; Cousins, I. T.; De Voogt, P.; Jensen, A. A.; Kannan, K.; Mabury, S. A.; van Leeuwen, S. P. Perfluoroalkyl and polyfluoroalkyl substances in the environment: terminology, classification, and origins. *Integrated Environmental Assessment and Management* **2011**, 7 (4), 513–541.
- (2) Glüge, J.; Scheringer, M.; Cousins, I. T.; DeWitt, J. C.; Goldenman, G.; Herzke, D.; Lohmann, R.; Ng, C. A.; Trier, X.; Wang, Z. An overview of the uses of per-and polyfluoroalkyl substances (PFAS). *Environmental Science: Processes & Impacts* **2020**, 22 (12), 2345–2373.
- (3) Evich, M. G.; Davis, M. J.; McCord, J. P.; Acrey, B.; Awkerman, J. A.; Knappe, D. R.; Lindstrom, A. B.; Speth, T. F.; Tebes-Stevens, C.; Strynar, M. J.; et al. Per-and polyfluoroalkyl substances in the environment. *Science* **2022**, *375* (6580), No. eabg9065.
- (4) Jiang, T.; Zhang, W.; Liang, Y. Uptake of individual and mixed per-and polyfluoroalkyl substances (PFAS) by soybean and their effects on functional genes related to nitrification, denitrification, and nitrogen fixation. *Sci. Total Environ.* **2022**, 838, 156640.
- (5) Jiang, T.; Geisler, M.; Zhang, W.; Liang, Y. Fluoroalkylether compounds affect microbial community structures and abundance of nitrogen cycle-related genes in soil-microbe-plant systems. *Ecotox Environ. Safe* **2021**, 228, 113033.
- (6) U.S. Environmental Protection Agency. *Drinking Water Health Advisories for GenX Chemicals and PFBS*. https://www.epa.gov/sdwa/drinking-water-health-advisories-genx-chemicals-and-pfbs (accessed July 28, 2022).
- (7) Schultz, M. M.; Barofsky, D. F.; Field, J. A. Fluorinated alkyl surfactants. *Environ. Eng. Sci.* **2003**, 20 (5), 487–501.
- (8) Zhang, W.; Zhang, Q.; Liang, Y. Ineffectiveness of ultrasound at low frequency for treating per-and polyfluoroalkyl substances in sewage sludge. *Chemosphere* **2022**, *286*, 131748.
- (9) Leung, S. C. E.; Shukla, P.; Chen, D.; Eftekhari, E.; An, H.; Zare, F.; Ghasemi, N.; Zhang, D.; Nguyen, N.-T.; Li, Q. Emerging technologies for PFOS/PFOA degradation: A review. *Sci. Total Environ.* **2022**, 827, 153669.
- (10) Zhang, D.; Zhang, W.; Liang, Y. Adsorption of perfluoroalkyl and polyfluoroalkyl substances (PFASs) from aqueous solution-A review. *Sci. Total Environ.* **2019**, *694*, 133606.
- (11) Zhang, W.; Jiang, T.; Liang, Y. Stabilization of per-and polyfluoroalkyl substances (PFAS) in sewage sludge using different sorbents. *Journal of Hazardous Materials Advances* **2022**, *6*, 100089.
- (12) Zhang, W.; Liang, Y. Performance of different sorbents toward stabilizing per-and polyfluoroalkyl substances (PFAS) in soil. *Environmental Advances* **2022**, *8*, 100217.
- (13) Sörengård, M.; Ostblom, E.; Köhler, S.; Ahrens, L. Adsorption behavior of per-and polyfluoralkyl substances (PFASs) to 44 inorganic and organic sorbents and use of dyes as proxies for PFAS sorption. *J. Environ. Chem. Eng.* **2020**, *8* (3), 103744.
- (14) Boyer, T. H.; Fang, Y.; Ellis, A.; Dietz, R.; Choi, Y. J.; Schaefer, C. E.; Higgins, C. P.; Strathmann, T. J. Anion exchange resin removal

- of per-and polyfluoroalkyl substances (PFAS) from impacted water: A critical review. Water Res. 2021, 200, 117244.
- (15) Dixit, F.; Dutta, R.; Barbeau, B.; Berube, P.; Mohseni, M. PFAS removal by ion exchange resins: A review. *Chemosphere* **2021**, 272, 129777.
- (16) Zhang, Q.; Deng, S.; Yu, G.; Huang, J. Removal of perfluorooctane sulfonate from aqueous solution by crosslinked chitosan beads: sorption kinetics and uptake mechanism. *Bioresource technology* **2011**, *102* (3), 2265–2271.
- (17) Zhou, Q.; Deng, S.; Yu, Q.; Zhang, Q.; Yu, G.; Huang, J.; He, H. Sorption of perfluorooctane sulfonate on organo-montmorillonites. *Chemosphere* **2010**, 78 (6), 688–694.
- (18) Zhao, L.; Bian, J.; Zhang, Y.; Zhu, L.; Liu, Z. Comparison of the sorption behaviors and mechanisms of perfluorosulfonates and perfluorocarboxylic acids on three kinds of clay minerals. *Chemosphere* **2014**, *114*, 51–58.
- (19) Sarkar, B.; Mandal, S.; Tsang, Y. F.; Kumar, P.; Kim, K.-H.; Ok, Y. S. Designer carbon nanotubes for contaminant removal in water and wastewater: a critical review. *Sci. Total Environ.* **2018**, *612*, 561–581
- (20) Xiao, X.; Ulrich, B. A.; Chen, B. L.; Higgins, C. P. Sorption of Poly- and Perfluoroalkyl Substances (PFASs) Relevant to Aqueous Film-Forming Foam (AFFF)-Impacted Groundwater by Biochars and Activated Carbon. *Environ. Sci. Technol.* **2017**, *51* (11), 6342–6351.
- (21) Bolan, N.; Sarkar, B.; Yan, Y.; Li, Q.; Wijesekara, H.; Kannan, K.; Tsang, D. C.; Schauerte, M.; Bosch, J.; Noll, H. Remediation of poly-and perfluoroalkyl substances (PFAS) contaminated soils-To mobilize or to immobilize or to degrade? *J. Hazard Mater.* **2021**, *401*, 123892.
- (22) Saha, D.; Khan, S.; Van Bramer, S. E. Can. porous carbons be a remedy for PFAS pollution in water? A perspective. *J. Environ. Chem. Eng.* **2021**, *9* (6), 106665.
- (23) Murray, C. C.; Marshall, R. E.; Liu, C. J.; Vatankhah, H.; Bellona, C. L. PFAS treatment with granular activated carbon and ion exchange resin: Comparing chain length, empty bed contact time, and cost. *Journal of Water Process Engineering* **2021**, *44*, 102342.
- (24) Zhang, R.; Yan, W.; Jing, C. Mechanistic study of PFOS adsorption on kaolinite and montmorillonite. *Colloids and surfaces*. **2014**, 462, 252–258.
- (25) Zhao, L. X.; Bian, J. N.; Zhang, Y. H.; Zhu, L. Y.; Liu, Z. T. Comparison of the sorption behaviors and mechanisms of perfluorosulfonates and, perfluorocarboxylic acids on three kinds of clay minerals. *Chemosphere* **2014**, *114*, 51–58.
- (26) Wang, F.; Liu, C. S.; Shih, K. M. Adsorption behavior of perfluorooctanesulfonate (PFOS) and perfluorooctanoate (PFOA) on boehmite. *Chemosphere* **2012**, *89* (8), 1009–1014.
- (27) Wang, F.; Shih, K. M. Adsorption of perfluorooctanesulfonate (PFOS) and perfluorooctanoate (PFOA) on alumina: Influence of solution pH and cations. *Water Res.* **2011**, *45* (9), 2925–2930.
- (28) Sarkar, B.; Xi, Y. F.; Megharaj, M.; Krishnamurti, G. S. R.; Bowman, M.; Rose, H.; Naidu, R. Bioreactive Organoclay: A New Technology for Environmental Remediation. *Crit Rev. Env Sci. Tec* **2012**, 42 (5), 435–488.
- (29) Uddin, F. Clays, nanoclays, and montmorillonite minerals. *Metallurgical and Materials Transactions A* **2008**, 39 (12), 2804–2814.
- (30) Zhou, Q.; He, H. P.; Zhu, J. X.; Shen, W.; Frost, R. L.; Yuan, P. Mechanism of p-nitrophenol adsorption from aqueous solution by HDTMA(+)-pillared montmorillonite Implications for water purification. *J. Hazard Mater.* **2008**, *154* (1–3), 1025–1032.
- (31) Wang, M. C.; Orr, A. A.; Jakubowski, J. M.; Bird, K. E.; Casey, C. M.; Hearon, S. E.; Tamamis, P.; Phillips, T. D. Enhanced adsorption of per- and polyfluoroalkyl substances (PFAS) by edible, nutrient-amended montmorillonite clays. *Water Res.* **2021**, *188*, 116534.
- (32) Kumar, B. S.; Dhakshinamoorthy, A.; Pitchumani, K. K10 montmorillonite clays as environmentally benign catalysts for organic reactions. *Catal. Sci. Technol.* **2014**, *4* (8), 2378–2396.
- (33) Kurwadkar, S.; Dane, J.; Kanel, S. R.; Nadagouda, M. N.; Cawdrey, R. W.; Ambade, B.; Struckhoff, G. C.; Wilkin, R. Per- and

- polyfluoroalkyl substances in water and wastewater: A critical review of their global occurrence and distribution. *Sci. Total Environ.* **2022**, 809, 151003.
- (34) Zhang, W.; Pang, S.; Lin, Z.; Mishra, S.; Bhatt, P.; Chen, S. Biotransformation of perfluoroalkyl acid precursors from various environmental systems: advances and perspectives. *Environ. Pollut.* **2021**, 272, 115908.
- (35) Zhang, W.; Cao, H.; Liang, Y. Plant uptake and soil fractionation of five ether-PFAS in plant-soil systems. *Sci. Total Environ.* **2021**, 771, 144805.
- (36) Fujii, S.; Polprasert, C.; Tanaka, S.; Lien, N. P. H.; Qiu, Y. New POPs in the water environment: distribution, bioaccumulation and treatment of perfluorinated compounds a review paper. *Journal of Water Supply Research and Technology-Aqua* **2007**, *56* (5), 313–326.
- (37) Steinle-Darling, E.; Reinhard, M. Nanofiltration for trace organic contaminant removal: Structure, solution, and membrane fouling effects on the rejection of perfluorochemicals. *Environ. Sci. Technol.* **2008**, 42 (14), 5292–5297.
- (38) PubChem. https://pubchem.ncbi.nlm.nih.gov/ (accessed August 7, 2022).
- (39) SGS. Physical and Chemical Properties of PFAS Compounds. https://www.sgs-ehsusa.com/wp-content/uploads/2018/09/Physical-and-Chemical-Properties-of-PFAS-compounds_vKFMH.pdf (accessed August 7, 2022).
- (40) Pauletto, P. S.; Bandosz, T. J. Activated carbon versus metalorganic frameworks: A review of their PFAS adsorption performance. *J. Hazard Mater.* **2022**, *425*, 127810.
- (41) Brooke, D.; Footitt, A.; Nwaogu, T.Environmental risk evaluation report: Perfluorooctanesulphonate (PFOS); 2004.
- (42) Abate, G.; Masini, J. C. Adsorption of atrazine, hydroxyatrazine, deethylatrazine, and deisopropylatrazine onto Fe (III) polyhydroxy cations intercalated vermiculite and montmorillonite. *J. Agr Food Chem.* **2005**, *53* (5), 1612–1619.
- (43) Brunauer, S.; Emmett, P. H.; Teller, E. Adsorption of gases in multimolecular layers. *J. Am. Chem. Soc.* **1938**, *60* (2), 309–319.
- (44) He, H. P.; Zhou, Q.; Martens, W. N.; Kloprogge, T. J.; Yuan, P.; Yunfei, X. F.; Zhu, J. X.; Frost, R. L. Microstructure of HDTMA(+)-modified montmorillonite and its influence on sorption characteristics. *Clays and Clay Minerals* **2006**, *54* (6), 689–696.
- (45) Chen, G. M.; Pan, J. J.; Han, B. X.; Yan, H. Adsorption of methylene blue on montmorillonite. *J. Dispersion Sci. Technol.* **1999**, 20 (4), 1179–1187.
- (46) Mizerska, U.; Fortuniak, W.; Rubinsztajn, S.; Chojnowski, J. Impact of cross-linker on the structure and hydrophilic-hydrophobic properties of polyhydromethylsiloxane-derived microspheres. *Polym. Advan Technol.* **2021**, 32 (10), 3967–3974.
- (47) Yan, B.; Munoz, G.; Sauvé, S.; Liu, J. Molecular mechanisms of per-and polyfluoroalkyl substances on a modified clay: a combined experimental and molecular simulation study. *Water Res.* **2020**, *184*, 116166.
- (48) Tzabar, N.; Ter Brake, H. Adsorption isotherms and Sips models of nitrogen, methane, ethane, and propane on commercial activated carbons and polyvinylidene chloride. *Adsorption* **2016**, 22 (7), 901–914.
- (49) Luft, C. M.; Schutt, T. C.; Shukla, M. K. Properties and Mechanisms for PFAS Adsorption to Aqueous Clay and Humic Soil Components. *Environ. Sci. Technol.* **2022**, *56* (14), 10053–10061.
- (50) Campos-Pereira, H.; Kleja, D. B.; Sjöstedt, C.; Ahrens, L.; Klysubun, W.; Gustafsson, J. P. The adsorption of per-and polyfluoroalkyl substances (PFASs) onto ferrihydrite is governed by surface charge. *Environ. Sci. Technol.* **2020**, *54* (24), 15722–15730.
- (51) Tang, C. Y.; Fu, Q. S.; Gao, D.; Criddle, C. S.; Leckie, J. O. Effect of solution chemistry on the adsorption of perfluorooctane sulfonate onto mineral surfaces. *Water Res.* **2010**, *44* (8), 2654–2662.
- (52) Grieco, S. A.; Chang, J.; Maio, E. Y.; Hwang, M. Comparing conventional and emerging adsorbents for per- and polyfluoroalkyl substances: Kinetic, equilibrium, and column experiments. *AWWA water science* **2021**, *3* (6), e1256.

- (53) Zhi, Y.; Liu, J. Adsorption of perfluoroalkyl acids by carbonaceous adsorbents: Effect of carbon surface chemistry. *Environ. Pollut.* **2015**, 202, 168–176.
- (54) Das, P.; Arias E, V. A.; Kambala, V.; Mallavarapu, M.; Naidu, R. Remediation of perfluorooctane sulfonate in contaminated soils by modified clay adsorbent—a risk-based approach. *Water, Air, & Soil Pollution* **2013**, 224 (12), 1–14.
- (55) Nwosu, F. O.; Ajala, O. J.; Owoyemi, R. M.; Raheem, B. G. Preparation and characterization of adsorbents derived from bentonite and kaolin clays. *Applied Water Science* **2018**, *8* (7), 195.
- (56) Segad, M.; Jonsson, B.; Åkesson, T.; Cabane, B. Ca/Na montmorillonite: structure, forces and swelling properties. *Langmuir* **2010**, 26 (8), 5782–5790.
- (57) Wu, C. Y.; Klemes, M. J.; Trang, B.; Dichtel, W. R.; Helbling, D. E. Exploring the factors that influence the adsorption of anionic PFAS on conventional and emerging adsorbents in aquatic matrices. *Water Res.* **2020**, *182*, 115950.
- (58) Xue, W.; He, H.; Zhu, J.; Yuan, P. FTIR investigation of CTAB-Al-montmorillonite complexes. *Spectrochimica Acta Part A: Molecular and Biomolecular Spectroscopy* **2007**, *67* (3–4), 1030–1036.
- (59) Abdel Ghafar, H. H.; Radwan, E. K.; El-Wakeel, S. T. Removal of hazardous contaminants from water by natural and zwitterionic surfactant-modified clay. *ACS omega* **2020**, *5* (12), 6834–6845.
- (60) Leite, S. T.; do Nascimento, F. H.; Masini, J. C. Fe (III)-polyhydroxy cations supported onto K10 montmorillonite for removal of phosphate from waters. *Heliyon* **2020**, *6* (4), No. e03868.
- (61) Hayati-Ashtiani, M. Characterization of nano-porous bentonite (montmorillonite) particles using FTIR and BET-BJH analyses. *Part Part Syst. Char* **2011**, 28 (3–4), 71–76.
- (62) Leite, S. T.; do Nascimento, F. H.; Masini, J. C. Fe(III)-polyhydroxy cations supported onto K10 montmorillonite for removal of phosphate from waters. *Heliyon* **2020**, *6* (4), e03868.
- (63) Hayati-Ashtiani, M. Characterization of Nano-Porous Bentonite (Montmorillonite) Particles using FTIR and BET-BJH Analyses. *Part Part Syst. Char* **2011**, 28 (3–4), 71–76.
- (64) Chen, Z.; Tian, H.; Li, H.; Li, J.; Hong, R.; Sheng, F.; Wang, C.; Gu, C. Application of surfactant modified montmorillonite with different conformation for photo-treatment of perfluorooctanoic acid by hydrated electrons. *Chemosphere* **2019**, 235, 1180–1188.
- (65) Rajeh, A.; Morsi, M.; Elashmawi, I. Enhancement of spectroscopic, thermal, electrical and morphological properties of polyethylene oxide/carboxymethyl cellulose blends: combined FT-IR/DFT. *Vacuum* **2019**, *159*, 430–440.
- (66) Housheh, S.; Trefi, S.; Chehna, M. F. Identification and Characterization of Prasugrel Degradation Products by GC/MS, FTIR and 1H NMR. Asian J. Pharm. Ana 2017, 7 (2), 55–66.
- (67) Kam, A.; Aroca, R.; Duff, J.; Tripp, C. P. Evolution of the Molecular Organization in Bis (n-propylimido) perylene Films under Thermal Annealing. *Chem. Mater.* **1998**, *10* (1), 172–176.
- (68) Chen, W.; Zhang, X.; Mamadiev, M.; Wang, Z. Sorption of perfluorooctane sulfonate and perfluorooctanoate on polyacrylonitrile fiber-derived activated carbon fibers: in comparison with activated carbon. *Rsc Adv.* **2017**, *7* (2), 927–938.
- (69) Fan, H.; Zhou, L.; Jiang, X.; Huang, Q.; Lang, W. Adsorption of Cu2+ and methylene blue on dodecyl sulfobetaine surfactant-modified montmorillonite. *Appl. Clay Sci.* **2014**, *95*, 150–158.
- (70) Hartvig, R. A.; van de Weert, M.; Ostergaard, J.; Jorgensen, L.; Jensen, H. Protein Adsorption at Charged Surfaces: The Role of Electrostatic Interactions and Interfacial Charge Regulation. *Langmuir* **2011**, *27* (6), 2634–2643.

NOTE ADDED AFTER ASAP PUBLICATION

This article originally published displaying an author's name incorrectly. Aswin Kumar Ilango's name is correctly displayed in the version published October 24, 2022.